UCSF

Title

Effect of microdistribution of alpha and beta-emitters in targeted radionuclide therapies on delivered absorbed dose in a GATE model of bone marrow

Permalink

Journal

ISSN

Authors

Tranel, Jonathan
Feng, Felix Y
St James, Sara
et al.

Publication Date

DOI

Peer reviewed

Effect of microdistribution of alpha and beta-emitters in targeted radionuclide therapies on delivered absorbed dose in a GATE model of bone marrow

Jonathan Tranel[1], **Felix Y. Feng**[2,3], **Sara St. James**[2], **Thomas A. Hope**[1,3]

[1.]Department of Radiology and Biomedical Imaging, University of California San Francisco, San Francisco CA, United States of America

[2.]Department of Radiation Oncology, University of California San Francisco, San Francisco CA, United States of America

[3.]UCSF Helen Diller Family Comprehensive Cancer Center, University of California San Francisco, San Francisco, CA, United States of America

Abstract

Acute hematologic toxicity is a frequent adverse effect of beta-emitter targeted radionuclide therapies (TRTs). Alpha emitters have the potential of delivering high linear energy transfer (LET) radiation to the tumor attributed to its shorter range. Antibody-based TRTs have increased blood-pool half-lives, and therefore increased marrow toxicity, which is a particular concern with alpha emitters. Accurate 3D absorbed dose calculations focusing on the interface region of blood vessels and bone can elucidate energy deposition patterns. Firstly, a cylindrical geometry model with a central blood vessel embedded in the trabecular tissue was modelled. Monte Carlo simulations in GATE were performed considering beta (^{177}Lu, ^{90}Y) and alpha emitters (^{211}At, ^{225}Ac) as sources restricted to the blood pool. Subsequently, the radioactive sources were added in the trabecular bone compartment in order to model bone marrow metastases infiltration (BMMI). Radial profiles, dose-volume histograms (DVHs) and voxel relative differences were used to evaluate the absorbed dose results. We demonstrated that alpha emitters have a higher localized energy deposition compared to beta emitters. In the cylindrical geometry model, when the sources are confined to the blood pool, the dose to the trabecular bone is greater for beta emitting radionuclides, as alpha emitters deposit the majority of their energy within 70 μm of the vessel wall. In the BMMI model, alpha emitters have a lower dose to untargeted trabecular bone. Our results suggest that when alpha emitters are restricted to the blood pool, as when labelled to antibodies, hematologic toxicities may be lower than expected due to differences in the microdistribution of delivered absorbed dose.

Keywords

cell-scale dosimetry; alpha emitters; bone marrow toxicities; targeted radionuclide therapy; Monte Carlo simulation

1. Introduction

The aim of targeted radionuclide therapy (TRT) is the destruction of tumors as a result of radiation delivered from radionuclides linked to molecules that selectively bind to the intended targets, often cell surface receptors that are overexpressed in tumors (Sgouros et al 2020). The molecular size of the targeting agents impacts their distribution. Large targeting agents, such as antibodies, have biologic half-lives of several days. Conversely, small molecules, such as peptides, have shorter biologic half-lives and often diffuse within tissues (Wadas et al 2014).

Beta emitters currently represent the majority of radionuclides employed in targeted radionuclide therapy and are well suited for the irradiation of large tumors since their range is several millimeters (Marcu *et al* 2018). However, the use of beta-emitting radionuclides may result in higher received radiation absorbed doses to normal tissues, specifically when an organ-at-risk (OAR) is close to the location of uptake, leading to the irradiation of normal cells. Alpha emitters deposit more energy per decay, with a linear energy transfer (LET) of ~100 keV μm^{-1}, which is greater by a factor 500 than the ~0.2 keV μm^{-1} LET of beta emitters. Furthermore, alpha particles have shorter ranges, below 100 μm (Mulford *et al* 2005). In the specific application of TRT, the relative biological effectiveness (RBE) for alpha particles is 5-fold that of the RBE of beta particles (Sgouros *et al* 2010). As a result, it has been suggested that alpha emitters are a superior choice for treating micrometastases, compared to beta emitters (Allen *et al* 2007, Elgqvist *et al* 2014).

These differences in absorbed dose deposition characteristics may be investigated using Monte Carlo simulations, accounting for the complexities of the absorbed dose distribution differences between radionuclides that decay via alpha or beta decay. These simulations may be used to inform future selection of radionuclide and targeting agent (small vs. large molecule) in clinical trials. Previous clinical experience has demonstrated toxicities from beta emitters to salivary glands, kidneys and bone marrow in TRT (Sweat *et al* 1998) in the setting of metastatic castration resistant prostate carcinoma (mCRPC). Moreover, bone marrow is often the absorbed dose-limiting organ across multiple TRTs (Sgouros *et al* 2010), and acute and chronic hematologic toxicities often prevent absorbed dose escalation. Finally, a diffuse infiltration of disease in the bone marrow may exclude patients from being treated with beta-emitter based TRT (Krachtowil *et al* 2016).

The choice of the labeled ligand is also critical. In the case of antibodies where the molecule is considerably larger than the small molecules employed in peptide-based TRTs, the prolonged intravascular half-life may result in more severe marrow injury as demonstrated with antibody-based mCRPC treatments, such as J591. In the Phase II study of ^{177}Lu-J591, the rates of Grade 3/4 marrow toxicities were greater than 50% (Tagawa *et al* 2013) and greater than 77% (Niaz *et al* 2020) for leukopenia, neutropenia or thrombocytopenia. Although clinical studies observed early evidence of clinical benefit of using ^{225}Ac instead of ^{177}Lu labeled to J591 (Tagawa *et al* 2020), there is significant concern for marrow toxicity, when labelling antibodies with alpha particles due to the increased local energy deposition compared to beta emitters. Small molecules are generally associated with better tumor-to-blood ratios due to faster tumor targeting and greater blood pool clearance than

antibodies (Wadas *et al* 2014). As a consequence of their fast clearance, small molecules labeled with short-range alpha particles may have increased sparing of OARs, in particular bone marrow, compared to when labeled with beta particles. Initial experience with [225]Ac-PSMA-617 has shown no significant increase in marrow toxicity compared to ^{177}Lu-labeled compounds, suggesting that the fast blood-pool clearance helps minimize injury to the marrow (Sathekge *et al* 2019). It is unclear how differences in microdistribution between antibodies and small molecules will impact marrow toxicity when using alpha emitters.

Most dosimetric studies refer to the mean absorbed dose at the organ level which might be a misleading index for quantifying biological effects especially for alpha emitters (Sgouros *et al* 2010). Although some alpha emitters have gamma, characteristic X-ray or bremsstrahlung emissions, no clinical imaging device is currently able to provide relevant uptake quantification at the scale of alpha emitters' range (Elgqvist *et al* 2014). Providing accurate absorbed dose calculations of the bone marrow is complicated by the inter-subject variability and tissue composition heterogeneity of the marrow (Sgouros *et al* 2000). Nonetheless, bone marrow models have been informative regarding the observed biological outcomes in the case of [223]Ra treatment for bone metastases in mCRPC (Henriksen *et al* 2003, Hobbs *et al* 2012, Pinto *et al* 2020).

In this work, we evaluate the impact of microdistribution of deposited energy within the trabecular bone compartment in order to better understand the potential distribution of marrow toxicity for alpha and beta emitters. Two situations were modelled: when the radionuclides are confined to the blood pool (as in the scenario of antibodies) or target metastatic sites in the trabecular bone so as to better understand potential toxicities associated with alpha and beta-labeled antibodies and small molecules. For this study, we evaluate two beta emitting radionuclides (^{177}Lu, ^{90}Y) and two alpha emitting radionuclides ([211]At, [225]Ac) using Monte Carlo simulations.

2. Materials & Methods

Monte Carlo (MC) simulations were performed using GATE (Geant4 Application for Tomographic Emission) version 9.0 (Sarrut *et al* 2014). A simple and a diffuse metastasis cylindrical model were evaluated. The absorbed dose distributions of ^{177}Lu, ^{90}Y, [211]At and [225]Ac were evaluated.

2.1 Simulation model

2.1.1 Cylindrical model—A bone marrow model was created with a blood vessel embedded in trabecular bone tissue (see Figure 1) with realistic dimensions (Steiniger *et al* 2016). The model is created with a voxel size of $10 \times 10 \times 10 \ \mu m^3$. This corresponds to each voxel having the approximate dimensions of a cell, with the assumption of a homogenous cell distribution (Hobbs *et al* 2012). The radionuclide sources were located in the "blood pool" compartment and the absorbed dose was calculated for each voxel (Henriksen *et al* 2003, Hobbs *et al* 2012, Pinto *et al* 2020). This model is composed of $61 \times 61 \times 61$ voxels, with a centered blood vessel compartment on the XY plane and symmetric along the Z axis, with a maximum diameter of 50 μm (5 voxels with a total of 793 voxels). It is worth noting that variations of vessel diameter have a minor effect on absorbed dose profile in trabecular

bone compartment from alpha and beta emitters (Falzone *et al* 2018). The blood vessel was embedded in a model of trabecular bone, considered as an organ at-risk (OAR). Both mass densities (blood: 1.06 g.cm^{-3}, trabecular bone (spongiosa): 1.05 g.cm^{-3}) and elemental compositions were extracted from the international commission on radiological protection (ICRP) male phantom data (Yeom *et al* 2016).

2.1.2   Diffuse bone marrow metastases infiltration—The second model evaluated diffuse bone marrow metastases infiltration (BMMI), which are common for both breast and prostate cancers (Coleman 2000). To model bone metastases and the impact of selecting an appropriate TRT, a total of fifty random voxels were designated as containing radioactivity in the trabecular bone compartment in the model, in addition to the blood pool (Figure 1b).

2.2   Radionuclides and simulation parameters

The absorbed dose deposition of four radioisotopes widely used in TRT were analyzed. Two are beta emitters: ^{177}Lu and ^{90}Y, with a respective maximum beta-emission range of 1.8 and 11.3 mm. The two other radionuclides are alpha emitters, ^{211}At, with a maximum alpha-emission range of 70 μm, and ^{225}Ac. ^{225}Ac has multiple alpha and beta particles generated in its decay chain, with a maximum alpha-emission range of 85 μm. Validation of these simulations was performed by comparing the results with those of Falzone et al (2018), ensuring that these results are consistent with those in the literature. The entire energy spectra and daughters were considered in the Monte Carlo models of the deposited radiation from these radionuclides. The selected number of primaries or disintegrations for alpha emitters was 10^6 and for beta emitters was 10^8. These numbers result in a relative uncertainty less than 2% at the center of the blood vessel for all the radionuclides. The model geometries were created using Python 3.6.9 in the .raw and .mhd formats that can be used as an input in GATE. The absorbed dose results generated with GATE (DoseActor) were visualized with 3D Slicer (Kikinis *et al* 2014). All Monte Carlo simulations were performed on a single CPU (3.3 GHz Intel Xeon W-2155), the *Livermore* physics model and the Mersenne-Twister engine were selected. This physics model considers all atomic shells, Auger electrons and has the best agreement with validation studies performed down to energies as low as 10 eV (Allison *et al* 2016). In the simulations, the step size limit or range cut-off parameter was chosen to be 1 μm, 1/10th of the voxel size. The model geometries were embedded in a world size of 10 cm. The GATE Radioactive Decay Module was enabled to ensure the full decay chain and its associated emissions were simulated, which is of particular interest for ^{225}Ac (Allison et al 2016, Pinto et al 2020).

2.3   Quantitative analysis

The absorbed dose deposition in the trabecular bone was evaluated for each radioisotope. The physical half-lives of these isotopes vary from 7.2 h (^{211}At) to 10 days (^{225}Ac). Biologic half-life is dependent on the selection of the targeting agent (small molecule or antibody) and introduces an added degree of freedom that is not considered in these simulations. The variation in physical half-lives and the potential variation in biological half-lives motivated the choice of presenting the results in absorbed dose per disintegration (Gy.Bq^{-1}.s^{-1}) or $D_{abs/d}$. All analyses were performed using radial absorbed dose profiles, cumulative dose-volume histograms (DVHs) and relative voxel differences.

2.3.1   Cylindrical model—Absorbed dose radial profiles as a function of distance from the center of the blood vessel were plotted for all the radioisotopes considering only radionuclide activity localized to the blood pool compartment. The center of the blood vessel is aligned with the axis origin. The trabecular bone compartment was segmented using a mathematical mask and DVHs were calculated and represent the absorbed dose delivered within the trabecular bone compartment. Consequently, the number of evaluated voxels for the trabecular compartment DVH is 226,188.

2.3.2   Diffuse bone marrow metastases infiltration (BMMI) model

2.3.2.1   Scaling absorbed dose distributions of beta emitters: The absorbed dose deposition characteristics (in particular the LET) between beta and alpha emitters lead to drastically different amounts of administered activity required to achieve the same biological effect. Data from clinical studies using alpha emitters injections show that these factors can vary from ~1.4 (^{177}Lu-DOTATOC at 29.6 GBq cumulative vs ^{213}Bi-DOTATOC at 21.6 GBq cumulative for neuroendocrine tumors, Marcu *et al* 2018) to ~770.8 (^{177}Lu-PSMA-617 at 14.8 GBq cumulative vs ^{225}Ac-PSMA-617 at 19.2 MBq cumulative for metastatic prostate cancer, Krachtowil et al, 2016). To account for this potential range, absorbed doses for the trabecular bone compartment were calculated for a broad range of relative injected activity: from 10^0 (same injected activity) to 10^3 (1 GBq of beta emitters versus 1 MBq of alpha emitters for example). DVHs were compared at different factors with relative activity for the alpha emitters remaining constant. Consequently, the number of evaluated voxels for the trabecular compartment DVH in the BMMI is 226,138.

2.3.2.2   Scaling of absorbed doses: Investigating the crossfiring effect of radioisotopes can be performed with analyzing the consequences of the specific distribution of the activity. Radioactive sources localized both in the blood pool and randomly at different sites was modelled within the trabecular bone (i.e. at different sites of metastasis). For beta and alpha emitters, the impact of crossfire will be different and quantifying these differences may help to highlight their respective efficiencies in the situation where diffuse metastases are widespread in the bone marrow.

Quantifying this discrepancy may determine how scaling of the absorbed dose in this situation may be approached. To this purpose, three absorbed dose maps from three different random distributions of the BMMI model were merged and compared to one distribution (Figure 2) which has the same number of metastases as in each of the three BMMI models, but with the local activity in each metastases scaled by a factor of three. In order to compare equal amounts of total radioactivity, the number of primaries for this latter distribution was respectively 3×10^6 and 3×10^8 for alpha and beta emitters. All distributions kept a total of fifty random source voxels (i.e. diffuse metastases) in the trabecular bone volume. A good agreement in this comparison would indicate that as activity increases in the source, the dose to the volume can be scaled linearly with the increase in activity. A poor agreement in this comparison would indicate that an increase in activity will not result in a scaled dose to the entire volume.

Comparisons were performed through an absorbed dose map of relative differences. An absorbed dose tolerance of 15% between the values was selected as the optimal compromise for highlighting differences between the radioisotopes as beta-emitters noise can hamper the analysis with lower tolerances at micrometric samplings. All the evaluated voxels pairs in the entire matrix having a relative difference less than 15% are considered as passing. As the 3D models matrix are using the same model and are therefore aligned, a relative difference is performed directly between voxels with the same coordinates as sources were defined manually.

3.   Results

All results are displayed in $D_{abs/d}$ (mGy Bq^{-1} s^{-1}) and presented for ^{177}Lu, ^{90}Y, ^{211}At and ^{225}Ac.

3.1   Cylindrical model

3.1.1   Radial profiles—Radial profiles for each of the radioisotopes were plotted in Figure 3, from 0 μm at the center of the blood vessel to 25 μm at the edge of the blood vessel, where the trabecular bone begins at 25 μm and extends to 300 μm.

At the origin (0 μm), ^{225}Ac $D_{abs/d}$ ratio is ~4 times greater than that of ^{211}At. Between alpha emitters and beta emitters, the magnitude order of absorbed dose deposition varies from 156 times (^{177}Lu $D_{abs/d}$ versus ^{211}At $D_{abs/d}$) to ~1 645 times (^{90}Y $D_{abs/d}$ versus ^{225}Ac $D_{abs/d}$). Among beta emitters, $D_{abs/d}$ for ^{177}Lu is ~3 times greater than ^{90}Y. In the trabecular bone, ^{211}At $D_{abs/d}$ is the lowest beyond 90 μm. As expected, the beta emitters activity needs to be multiplied by ~250–1 000 in order to achieve the same absorbed dose as ^{211}At and ^{225}Ac in the blood vessel.

In the trabecular bone compartment, 99.9% of the energy of ^{211}At is deposited within 90 μm and within 100 μm for ^{225}Ac. At 300 μm, 99.6% of the energy of ^{177}Lu is deposited and 98.3% for ^{90}Y. The highest mean kinetic energy of beta-emission (933.1 keV) is associated with ^{90}Y and is consistent with a lower energy deposition at the center of the blood vessel as particles have the longest range.

In order to relate our results with the bone marrow histology, data from (Bourke *et al* 2009) were extracted in regards to the relative frequency of hematopoietic progenitor cells based on the distance from the blood vessel wall. For clarity purposes, results from Figure 3 were normalized with the maximum $D_{abs/d}$ of ^{225}Ac located at the center of the blood vessel, visible in Figure 4.

According to (Bourke *et al* 2009) data, 25% of the hematopoietic cells are located within 100 μm of the nearest vessel. When extrapolated to our results, 75% of these cells receive minimal absorbed dose from by alpha emitters restricted to the blood vessel. This results in a 10^3-10^4 fold decrease absorbed dose to marrow progenitor cells compared to beta emitters.

3.1.2 Dose Volume Histograms—DVHs of the trabecular bone compartment for each of the radioisotopes were plotted in Figure 5, normalized with the maximum ^{225}Ac $D_{abs/d}$ located at the center of the blood vessel.

As shown in Figure 5, ^{225}Ac and ^{211}At spare most of the trabecular bone volume, as demonstrated by the L-shape of the DVH curve. ^{225}Ac has a maximum absorbed dose of 0.02 mGy Bq^{-1} s^{-1} for more than 95% of the trabecular bone volume ($D_{5\%}$), while ^{211}At has the lowest irradiation for the whole volume with a $D_{5\%}$ equal to 0.01 mGy Bq^{-1} s^{-1}. In comparison, the $D_{5\%}$ for ^{177}Lu and ^{90}Y is roughly 10-fold higher at 0.15 and 0.22 mGy Bq^{-1} s^{-1} respectively.

3.2 BMMI model

3.2.1 Dose Volume Histograms—DVHs of the trabecular bone compartment with the BMMI model for each of the radioisotopes normalized with the maximum ^{225}Ac $D_{abs/d}$ located at the center of the blood vessel are shown in Figure 6.

Radioactive sources directly located in the trabecular bone compartment lead to greater increase in irradiation from alpha emitters (^{211}At, ^{225}Ac) compared to beta emitters (^{177}Lu, ^{90}Y), although alpha emitters still have an overall lower absorbed dose to the trabecular bone compartment. ^{225}Ac $D_{5\%}$ increase to 0.03 mGy Bq^{-1} s^{-1} and ^{211}At $D_{5\%}$ to 0.02 mGy Bq^{-1} s^{-1} (respectively +50% and +100% in regards to the cylindrical model, see 3.1.2). Conversely, ^{177}Lu and ^{90}Y $D_{5\%}$ variations are negligible.

3.2.2 Scaling absorbed dose distributions of beta emitters—DVHs of the trabecular bone compartment with the BMMI model were plotted in Figure 7 for injected activity factors of beta emitters varying from 10^0 (equivalent activity) to 10^3. Each radioisotope is displayed in $D_{abs/d}$, reflecting the differences of injected activity between alpha and beta emitters.

DVHs at different injected activity factors of beta emitters show that the absorbed dose in the trabecular bone compartment is greater with beta emitters than alpha emitters from an injected activity factor of 10^2 and larger. The ^{177}Lu and ^{90}Y $D_{5\%}$ values to the trabecular bone compartment from beta emitters are near 0.02 mGy Bq^{-1} s^{-1} at a ratio of 100:1, and logically increase to 0.2 mGy Bq^{-1} s^{-1} at 1 000:1. For noting, ^{225}Ac and ^{211}At $D_{5\%}$ respectively remained equal to 0.03 mGy Bq^{-1} s^{-1} and 0.02 mGy Bq^{-1} s^{-1}.

3.2.3 Scaling of absorbed doses—Maps of $D_{abs/d}$ and relative differences are displayed in Figure 8 for an example transverse slice in the middle of the volume. The calculated percentage of voxels having relative differences lower than 15% is applied to the whole volume for each radioisotope.

The blood vessel area at the center of the model is in agreement for all isotopes as there is a high concentration of the radionuclides in this region and when it is scaled there is no variation (i.e. the scaled model agrees with the sum of the individual simulations). For the trabecular bone compartment, visualization and passing (15%) percentage demonstrate that ^{90}Y absorbed dose deposition is the least impacted by the scaling of activity within diffuse

metastases with 96.6% of voxels in the scaled model within ±15% of the absorbed dose of the additive model. The highest passing (15%) percentage correspond to the radionuclide with the least local energy deposition, i.e. the beta emitters. Conversely, ^{211}At and ^{225}Ac have lower passing (15%) percentages (13.2% and 24.7%) compared to beta emitters, which is caused by the local energy deposition seen with alpha emitters. Higher passing (15%) percentages indicate the ability for the results to be scaled, while lower passing (15%) percentages indicate that a simple scaling cannot be used.

4. Discussion

In this work, Monte Carlo simulations of four radionuclides of interest for the field of TRT are presented. These included two isotopes that decay via beta decay (^{177}Lu and ^{90}Y) along with two isotopes that decay via alpha decay (^{211}At and ^{225}Ac). Both simplistic and more complex geometries were evaluated to expand the current understanding of how these radionuclides may be used therapeutically, with a focus on understanding how the energy deposited from radionuclides in the blood pool (vessels) impacts the absorbed dose to the regions where bone marrow progenitor cells are formed. The radiation absorbed dose to these cells in TRT often are a limiting factor for these therapies.

When the sources are confined to the blood pool, the absorbed dose to the trabecular bone is greater for beta emitting radionuclides. In the cylindrical geometry when the sources are confined to the blood vessel, the most $D_{abs/d}$ sparing effect is observed with ^{211}At in the trabecular bone compartment for the furthest located cells from the sources, beyond 100 μm. ^{225}Ac delivers the highest irradiation to the trabecular bone volume per disintegration but has a rapid decrease in absorbed dose deposition (factor of 3 631x at 100 μm, compared to 13–20x for ^{90}Y-^{177}Lu).

This highlights the need to minimize the duration of time that beta emitting radionuclides are in the blood pool, which in clinical practice has been achieved by using small molecules with fast renal clearance. For alpha emitting radionuclides, the absorbed dose to the trabecular bone drops off quickly with increasing distance from the vessel wall, as the range of alphas ensures absorbed dose is minimal at distances greater than 100 μm. For example, 30% of the hematopoietic cells in the iliac crest are located within 70 μm of the blood vessel wall (Watchman *et al* 2007), meaning that 70% of marrow progenitor cells would receive minimal absorbed dose from alpha emitters located in the blood pool. This percentage slightly varies with (Bourke *et al* 2009) stating that 25% of the hematopoietic cells are within the 70 μm distance of the blood vessel wall.

Antibodies are generally restricted to the blood pool as they do not freely diffuse into the interstitial space due to their molecular size. With antibodies labeled to beta emitters, marrow toxicity is particularly concerning due to the prolonged blood pool residence time, which can last up to several days (Lobo *et al* 2004). Our results suggest that this can be mitigated by labelling antibodies with alpha emitters, which when localized to the blood pool spare the majority of marrow progenitor cells. Recent clinical studies (Tagawa *et al* 2020) observed a better bone marrow tolerance with the use of ^{225}Ac compared to ^{177}Lu when labeled to the J591 antibody, in agreement with what our results would predict.

The agreement of the cylindrical model to the results of other groups (Henriksen *et al* 2003, Hobbs *et al* 2012, Pinto *et al* 2020, Falzone *et al* 2018) gives confidence in the Monte Carlo simulation implementation and the analysis tools used. For the beta emitters, the higher LET of ^{177}Lu results in a higher local energy deposition than ^{90}Y. For the alpha emitters, the relative measured $D_{abs/d}$ in our model was four times lower for ^{211}At compared to ^{225}Ac, which is consistent with the fact that the decay scheme of ^{225}Ac results in four alpha particles emitted in total, compared to the one emitted alpha-particle for ^{211}At.

The cylindrical model was then extended to include the presence of diffuse radioactive sources in the trabecular bone compartment. In this geometry, an overall increase of the $D_{abs/d}$ is observed for alpha emitters whereas variations are negligible for betas emitters, confirming their non-specificity for diffuse metastases. Although the interpretation of the DVH metrics reflect a higher sparing effect with the use of alpha in regard to beta emitters, information about spatial and local variations are not pinpointed.

One final way to illustrate the localized absorbed dose deposition of alpha emitters is the ability to scale the results of the BMMI model. The scaling study was performed by comparing the sum of three different random models of metastases with a scaled model. The agreement seen for the beta emitters in the scaled scenarios show good agreement with the sum of three distinct patterns of metastasis with the absorbed dose to the healthy portions of the bone increase linearly due to the relatively large range of the beta emitting radionuclides. In contrast, there was poor agreement seen in the scenario where alpha emitters were evaluated. This indicates that in the presence of diffuse metastasis, treatment with alpha emitting radionuclides results in lower absorbed dose to untargeted trabecular bone.

These results show that when modelling absorbed dose deposition with alpha emitters, Monte Carlo modeling with absorbed dose distributions are important at the scale of micrometers, which are not typically required when evaluating beta emitters. Nevertheless, our simplistic model assumed a homogeneous cell distribution of 10 μm and do not consider the replacement of the pluripotent cells with various lineage in the bone marrow (Henriksen *et al* 2003).

SPECT/CT, which images gamma photons, is commonly used to localize activity with beta emitters, although SPECT is limited as it has a spatial resolution greater than 1 cm. With alpha emitters, regardless of the algorithm used for the absorbed dose calculations, establishing an absorbed dose-effect relationship is not feasible as demonstrated with the observed biological miscorrelations when calculating the absorbed dose based on clinical scintigraphic images (Chiesa *et al* 2019). Hence, absorbed dose calculations at the micrometric scale when using alpha emitters is the only way for predicting associated toxicities in bone marrow.

5. Conclusion

Our results demonstrate that when alpha emitters are localized to the blood pool, they result in relative sparing of bone marrow progenitor cells relative to beta emitters. This work ties together simulations with clinical experiences to highlight the importance of the interplay of

the targeting molecule (antibodies or small molecules) and the chosen radionuclide (alpha or beta emitting radionuclides). While beta-emitting radionuclides, when linked to larger molecules (antibodies), can result in significant marrow exposure, alpha particles may result in minimal toxicity due to their short particle length. Overall the local energy deposition characteristics of alpha emitters necessitates absorbed dose simulations performed at the cellular scale to better understand the spatial distribution of the absorbed dose.

Acknowledgements

References

Allen BJ, Raja C, Rizvi S, Song EY and Graham P 2007 Tumour anti-vascular alpha therapy: A mechanism for the regression of solid tumours in metastatic cancer Phys. Med. Biol 52

Allison J et al. 2016 Recent developments in GEANT4 Nucl. Instruments Methods Phys. Res. Sect. A Accel. Spectrometers, Detect. Assoc. Equip 835 186–225

Bourke VA, Watchman CJ, Reith JD, Jorgensen ML, Dieudonnè A and Bolch WE 2009 Spatial gradients of blood vessels and hematopoietic stem and progenitor cells within the marrow cavities of the human skeleton Blood 114 4077–80 [PubMed: 19749092]

Chiesa C, Bardiès M and Zaidi H 2019 Voxel-based dosimetry is superior to mean absorbed dose approach for establishing dose-effect relationship in targeted radionuclide therapy Med. Phys 46 5403–6 [PubMed: 31584697]

Coleman RE 2000 Metastatic bone disease: clinical features,pathophysiology and treatment strategies Cancer Treat. Rev 27 165–76

Elgqvist J, Frost S, Pouget JP and Albertsson P 2014 The potential and hurdles of targeted alpha therapy - clinical trials and beyond Front. Oncol 4 1 1–9 [PubMed: 24478982]

Falzone N et al. 2018 Dosimetric evaluation of radionuclides for VCAM-1- targeted radionuclide therapy of early brain metastases Theranostics 8 292–303 [PubMed: 29290808]

Henriksen G, Fisher DR, Roeske JC, Bruland Ø S and Larsen RH 2003 Targeting of osseous sites with alpha-emitting 223Ra: comparison with the beta-emitter 89Sr in mice. J. Nucl. Med 44 252–9 [PubMed: 12571218]

Hobbs RF, Song H, Watchman CJ, Bolch WE, Aksnes AK, Ramdahl T, Flux GD and Sgouros G 2012 A bone marrow toxicity model for 223Ra alpha-emitter radiopharmaceutical therapy Phys. Med. Biol 57 3207–22 [PubMed: 22546715]

Kikinis R, Pieper SD and Vosburgh KG 2014 3D Slicer: A Platform for Subject-Specific Image Analysis, Visualization, and Clinical Support Intraoperative Imaging and Image-Guided Therapy ed Jolesz FA (New York, NY: Springer New York) pp 277–89

Kratochwil C, Bruchertseifer F, Giesel FL, Weis M, Verburg FA, Mottaghy F, Kopka K, Apostolidis C, Haberkorn U and Morgenstern A 2016 225Ac-PSMA-617 for PSMA-targeted a-radiation therapy of metastatic castration-resistant prostate cancer *J.* Nucl. Med 57 1941–4

Lobo ED, Hansen RJ and Balthasar JP 2004 Antibody pharmacokinetics and pharmacodynamics *J.* Pharm. Sci 93 2645–68

Low DA, Harms WB, Mutic S and Purdy JA 1998 A technique for the quantitative evaluation of dose distributions. Med. Phys 25 656–61 [PubMed: 9608475]

Marcu L, Bezak E and Allen BJ 2018 Global comparison of targeted alpha vs targeted beta therapy for cancer: In vitro, in vivo and clinical trials Crit. Rev. Oncol. Hematol 123 7–20 [PubMed: 29482781]

Mulford DA, Scheinberg DA and Jurcic JG 2005 The promise of targeted {alpha}-particle therapy. J. Nucl. Med 46 Suppl 1 199S–204S [PubMed: 15653670]

Niaz MJ, Skafida M, Osborne J, Nanus D, Molina A, Thomas C, Vallabhajosula S, Christos P, Bander N and Tagawa S 2020 Comparison of prostate-specific membrane antigen (PSMA)-targeted radionuclide therapy (TRT) with lutetium-177 (177Lu) via antibody J591 vs small molecule ligand PSMA-617 J. Urol 203 e367–e367

Pinto GM, Bonifacio DAB, de Sá LV., Lima LFC, Vieira IF and Lopes RT 2020 A cell-based dosimetry model for radium-223 dichloride therapy using bone micro-CT images and GATE simulations Phys. Med. Biol 65 045010 [PubMed: 31935695]

Sathekge M, Bruchertseifer F, Knoesen O, Reyneke F, Lawal I, Lengana T, Davis C, Mahapane J, Corbett C, Vorster M and Morgenstern A 2019 225Ac-PSMA-617 in chemotherapy-naive patients with advanced prostate cancer: a pilot study Eur. J. Nucl. Med. Mol. Imaging 46 129–138 [PubMed: 30232539]

Sarrut D. et al. 2014; A review of the use and potential of the GATE Monte Carlo simulation code for radiation therapy and dosimetry applications. Med. Phys. 41

Sgouros G, Stabin M, Erdi Y, Akabani G, Kwok C, Brill AB and Wessels B 2000 Red marrow dosimetry for radiolabeled antibodies that bind to marrow, bone, or blood components Med. Phys 27 2150–64 [PubMed: 11011745]

Sgouros G et al. 2010 MIRD pamphlet No. 22 (Abridged): Radiobiology and dosimetry of α-particle emitters for targeted radionuclide therapy J. Nucl. Med 51 311–28 [PubMed: 20080889]

Steiniger BS, Stachniss V, Wilhelmi V, Seiler A, Lampp K, Neff A, Guthe M and Lobachev O 2016 Three-dimensional arrangement of human bone marrow microvessels revealed by immunohistology in undecalcified sections PLoS One 11 1–25

Sweat SD, Pacelli A, Murphy GP and Bostwick DG 1998 Prostate-specific membrane antigen expression is greatest in prostate adenocarcinoma and lymph node metastases Urology 52 637–40 [PubMed: 9763084]

Tagawa ST et al. 2013 Phase II study of lutetium-177-labeled anti-prostate-specific membrane antigen monoclonal antibody J591 for metastatic castration-resistant prostate cancer Clin. Cancer Res 19 5182–91 [PubMed: 23714732]

Tagawa ST et al. 2020 Dose-escalation results of a phase I study of 225Ac-J591 for progressive metastatic castration resistant prostate cancer (mCRPC). J. Clin. Oncol 38 114

Yeom YS et al. 2016 Development of skeletal system for mesh-type ICRP reference adult phantoms Phys. Med. Biol 61 7054–73 Online: 10.1088/0031-9155/61/19/7054 [PubMed: 27648514]

Wadas Thaddeus J., Pandya Darpan N., Kumar Kiran Solingapuram Sai AM 2014 Molecular Targeted α-Particle Therapy for Oncologic Applications AJR Am J Roentgenol. 203 253–60 [PubMed: 25055256]

Watchman CJ, Bourke VA, Lyon JR, Knowlton AE, Butler SL, Grier DD, Wingard JR, Braylan RC and Bolch WE 2007 Spatial distribution of blood vessels and CD34+ hematopoietic stem and progenitor cells within the marrow cavities of human cancellous bone J. Nucl. Med 48 645–54 [PubMed: 17401104]
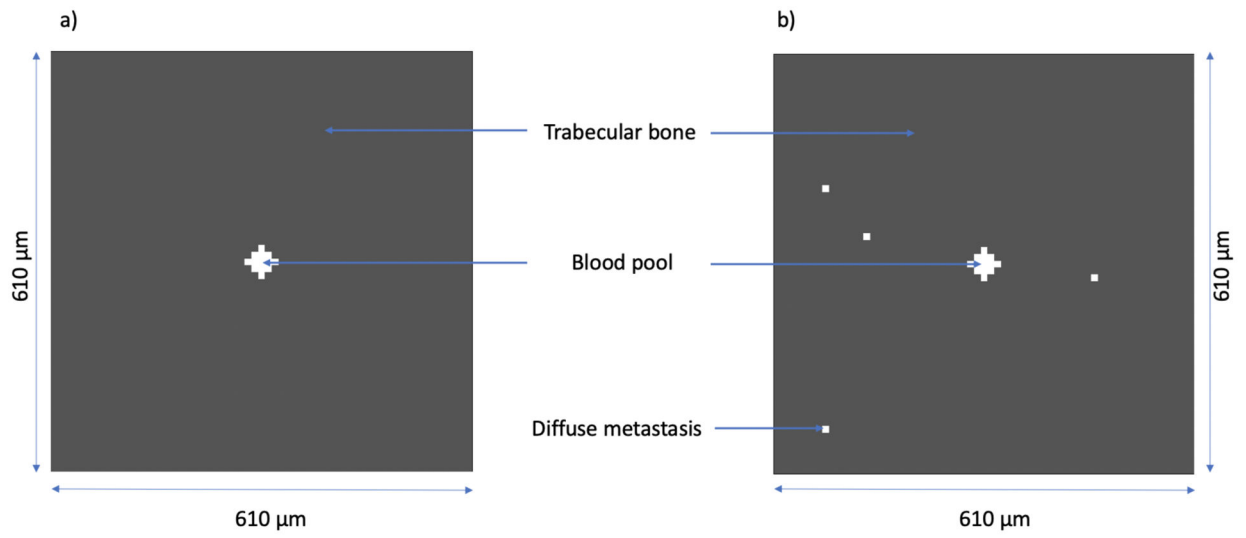
Figure 1 –.
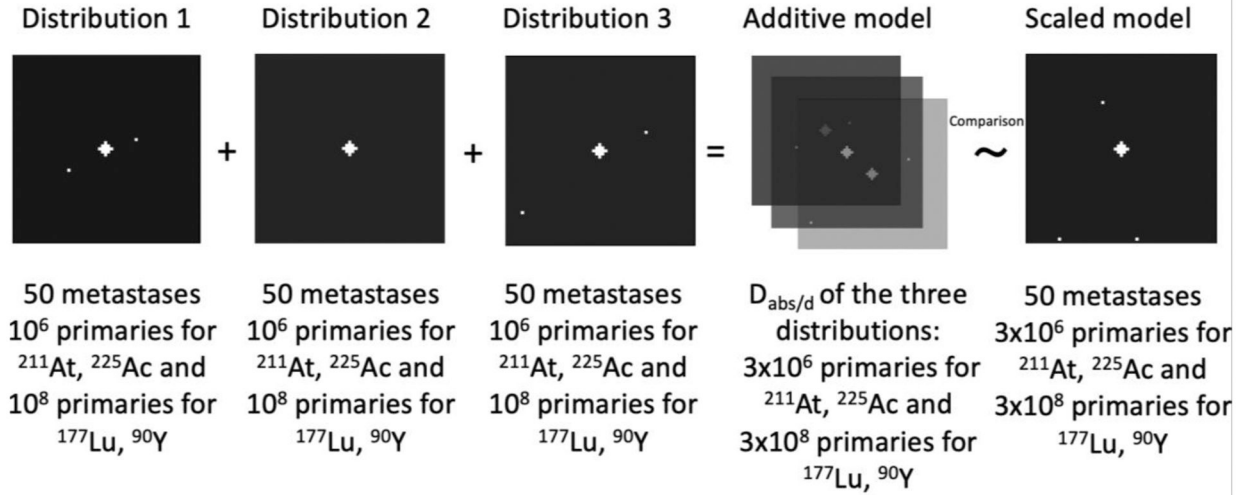Transversal slice of (a) the cylindrical bone marrow model and (b) the BMMI model.

Figure 2 -

Transversal slices of the BMMI model with four different random distributions. The three resulting absorbed dose (10^6 or 10^8 each) maps were merged (left) and compared to the scaled (3×10^6 or 3×10^8) one (right).
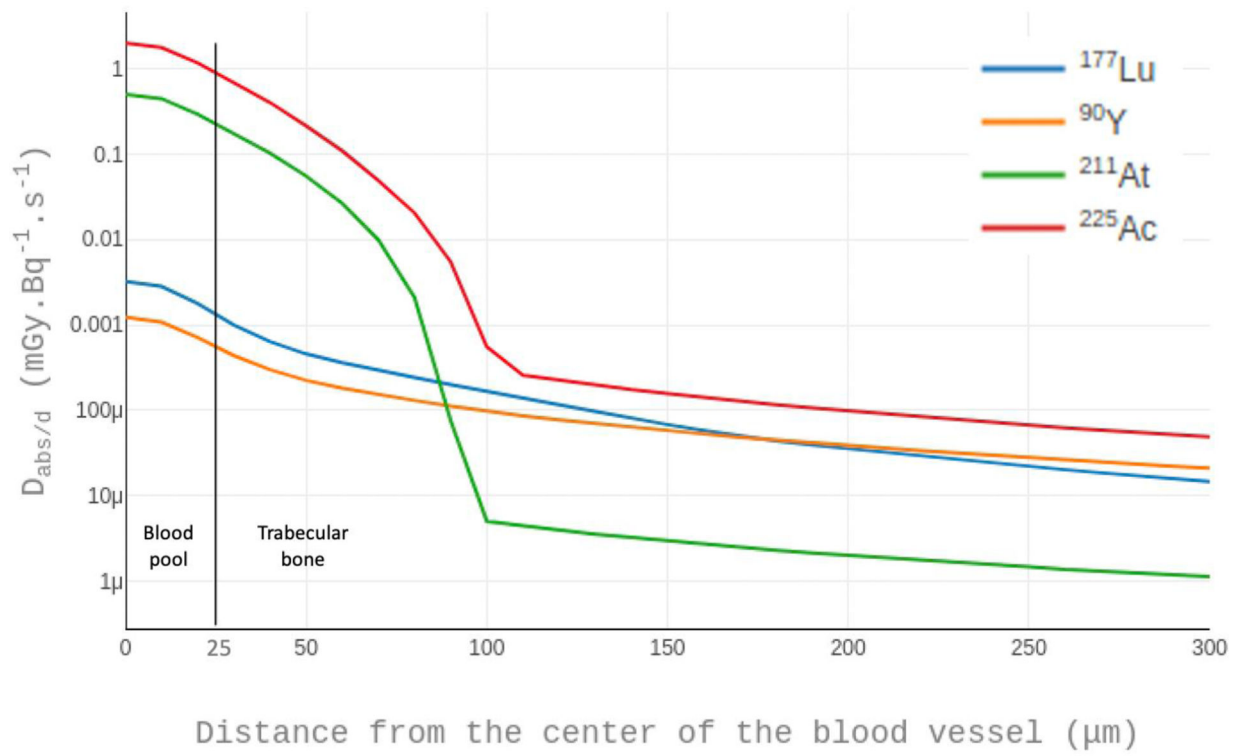
Figure 3 -
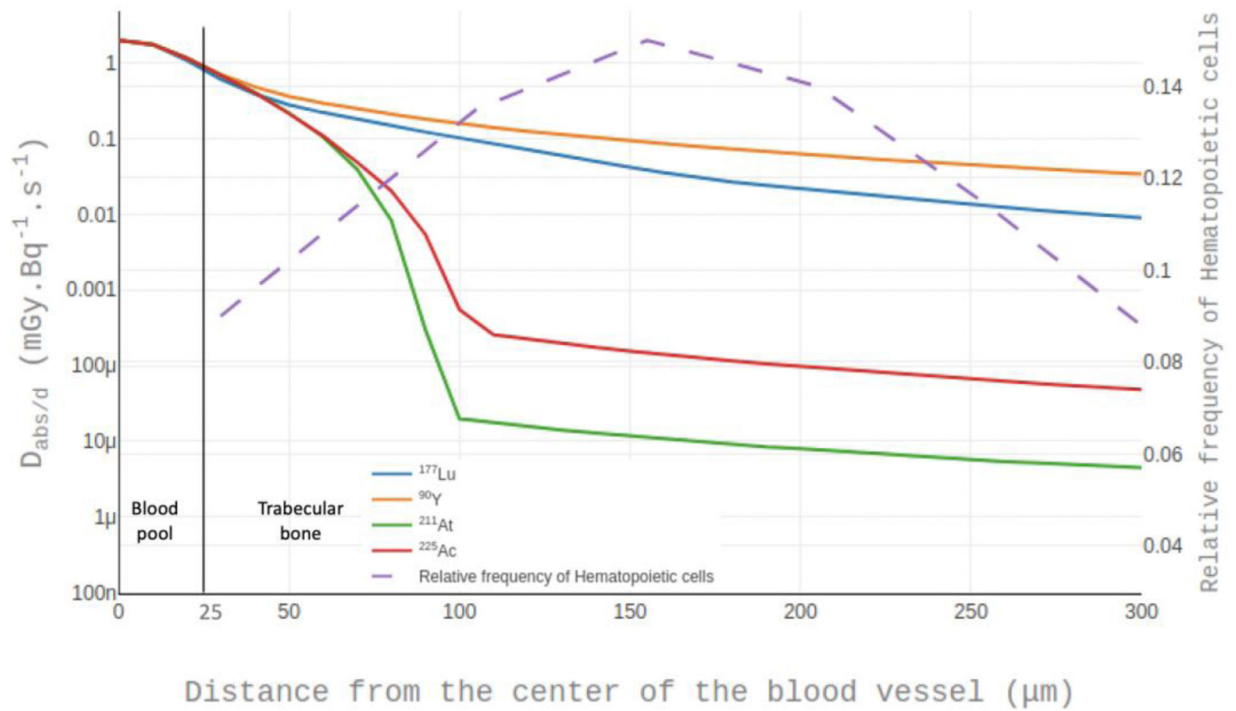Radial profiles from the cylindrical model of the absorbed dose per disintegration for the radioisotopes

Figure 4 –.
Normalized radial profiles of absorbed dose superimposed to the relative frequency of hematopoietic cells by distance from the center of the blood vessel.
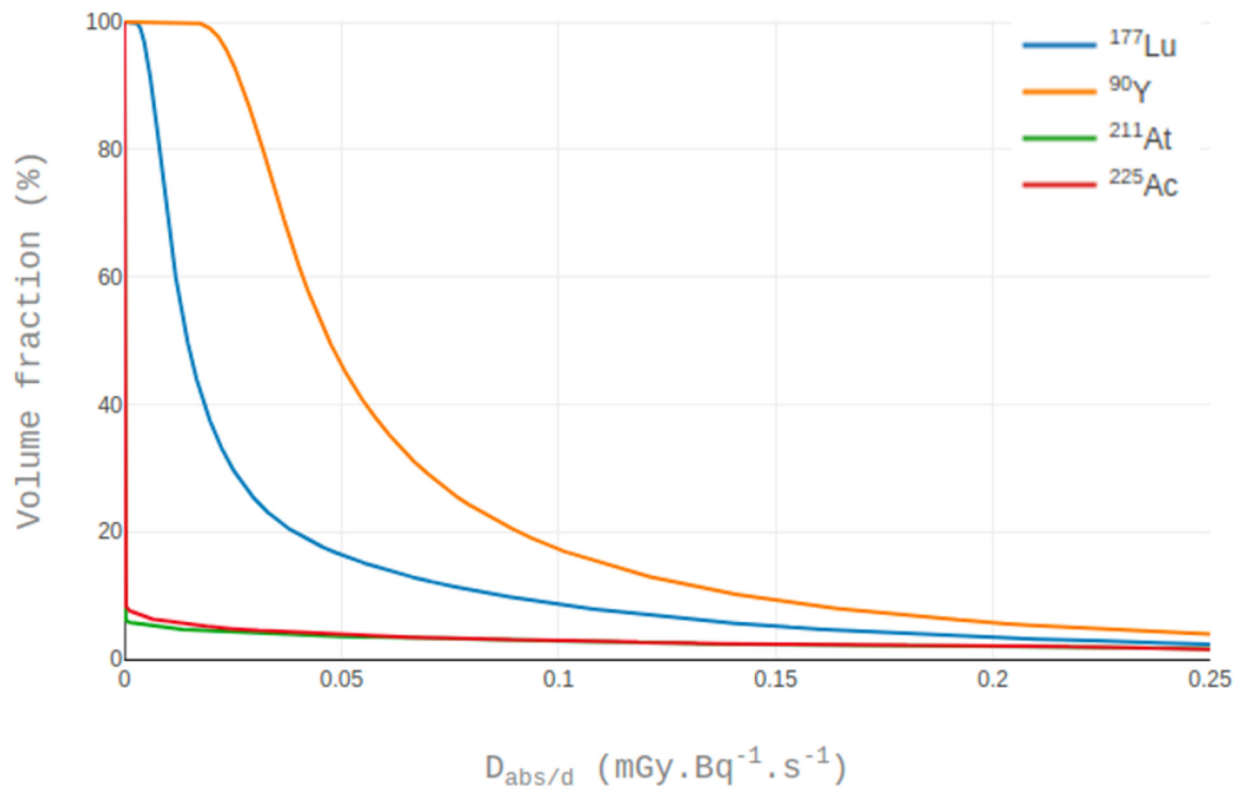
Figure 5 -
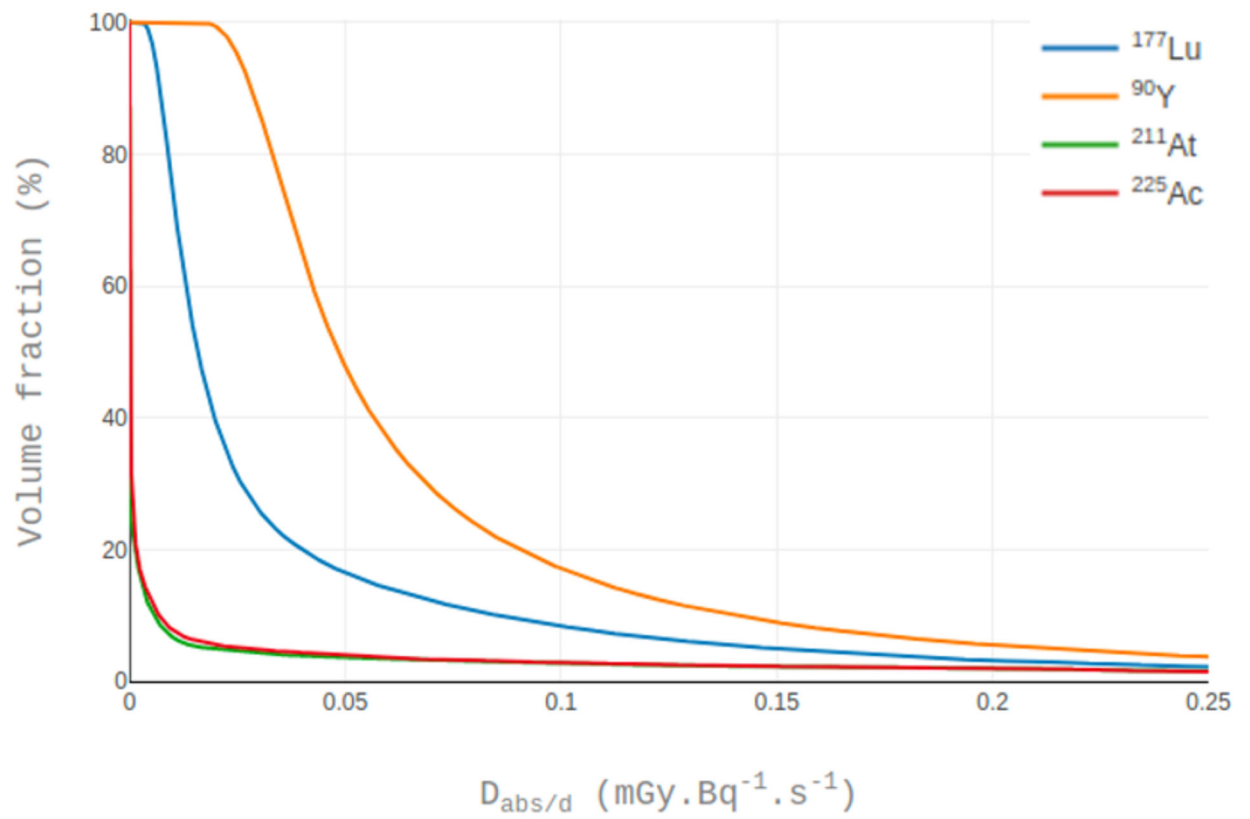Dose Volume Histogram of trabecular bone compartment for the cylindrical model

Figure 6 -
Dose volume histograms of the trabecular bone compartment for the BMMI model
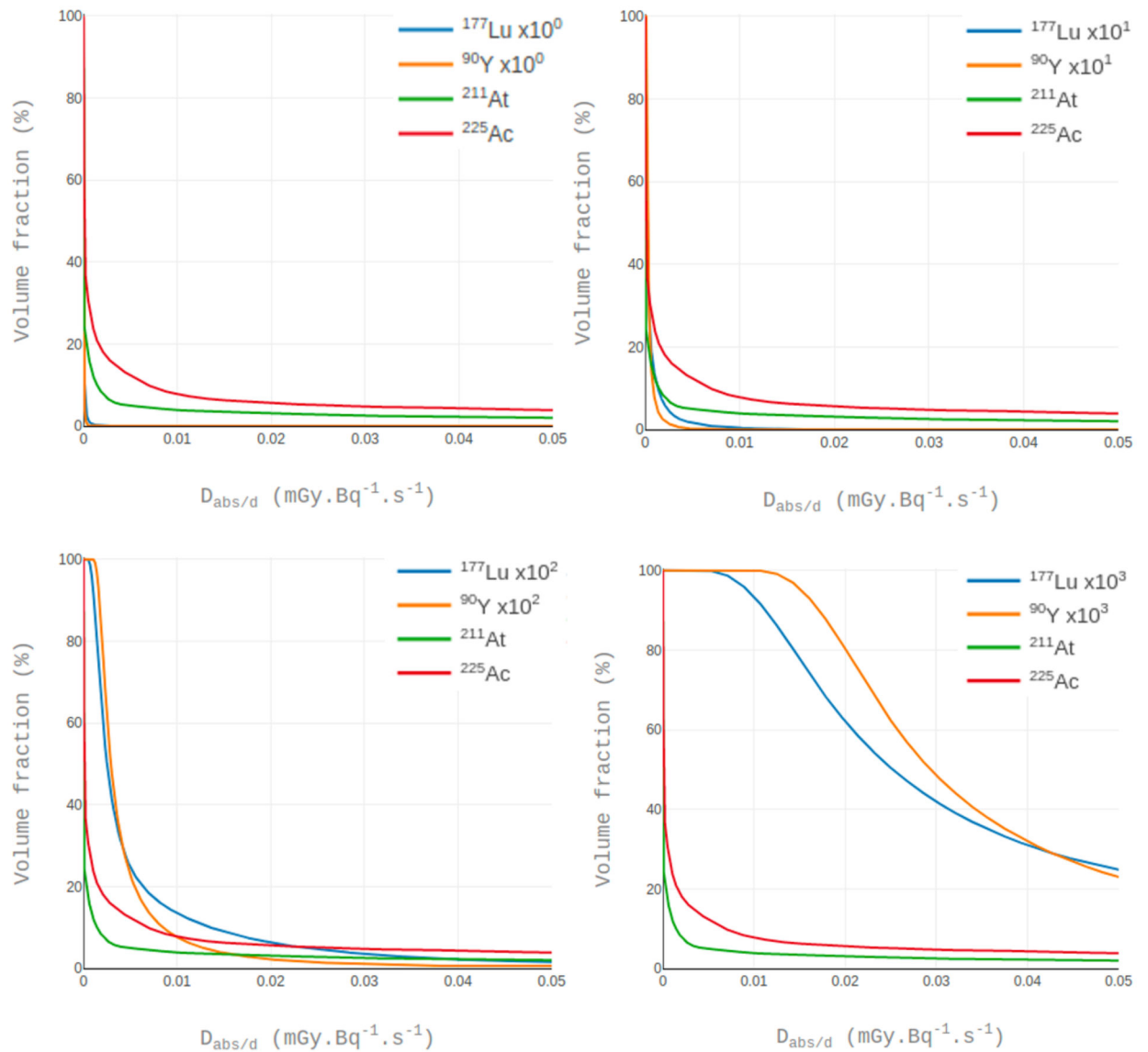
Figure 7 -

Dose volume histograms of the trabecular bone compartment for the BMMI model with increasing levels of injected activity factor for beta emitters from 10^0 (upper left) to 10^3 (lower right).
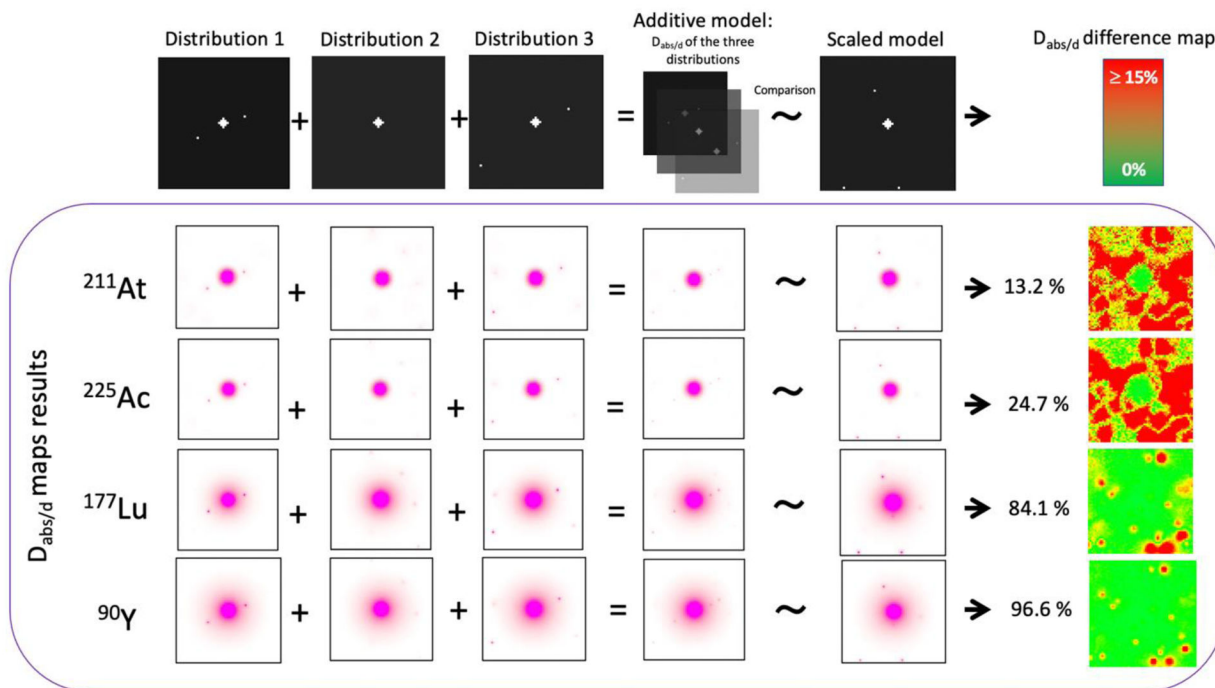
Figure 8 -

Transversal slices of maps showing the $D_{abs/d}$ and relative differences. Voxels with small differences (15%) are colored in green, greater differences (>15%) in red. The passing percentage (voxels having 15% of relative differences) in the marrow compartment provided next to each image (%)